Spiral surface plasmon modes inside metallic nanoholes

Chih-Min Chen,[1,2,3] Jian-Liang Ke,[2,3] Yung-Chiang Lan,[1,*] and Ming-Che Chan[2,4]

[1]*Department of Photonics, National Cheng Kung University, Tainan City 70101, Taiwan*
[2]*College of Photonics, National Chiao-Tung University, Tainan City 71150, Taiwan*
[3]*Each author contributed equally to this work*
[4]*mcchan@nctu.edu.tw*
[*]*lanyc@mail.ncku.edu.tw*

Abstract: Spiral surface plasmon (SSP) modes that propagate inside a silver (Ag) nanohole are investigated by performing both simulations and theoretical analyses. The SSP modes are formed by a linear combination of two rotating SP eigenmodes of the Ag nanohole in the fast-wave branch. Inside a uniform Ag nanohole, the handedness and the number of strands of the SSP modes are determined by both the component SP eigenmodes and their rotation directions. The spiral pitch of the SSP mode increases with the nanohole radius for a fixed wavelength and is inversely related to the incident wavelength for a fixed nanohole radius. Inside a tapered Ag nanohole, the spiral pitch decreases with the reduction of nanohole radius. However, the azimuth-integrated field energy density increases to a maximum value and then falls. For a tapered Ag-clad fiber capped by a tapered Ag nanorod, the SSP mode reverses its handedness when it passes through the fiber-nanorod interface. Furthermore, using this composite structure, the field energy density of SSP mode that arrives at the tip of the tapered nanorod is largely increased.

OCIS codes: (240.6680) Surface plasmons; (250.5403) Plasmonics; (230.7370) Waveguides; (130.2790) Guided waves.

References and links

1. T. W. Ebbesen, H. J. Lezec, H. F. Ghaemi, T. Thio, and P. A. Wolff, "Extraordinary optical transmission through sub-wavelength hole arrays," Nature **391**(6668), 667–669 (1998).
2. H. F. Ghaemi, T. Thio, D. E. Grupp, T. W. Ebbesen, and H. J. Lezec, "Surface plasmons enhance optical transmission through subwavelength holes," Phys. Rev. B **58**(11), 6779–6782 (1998).
3. L. Martín-Moreno, F. J. García-Vidal, H. J. Lezec, K. M. Pellerin, T. Thio, J. B. Pendry, and T. W. Ebbesen, "Theory of extraordinary optical transmission through subwavelength hole arrays," Phys. Rev. Lett. **86**(6), 1114–1117 (2001).
4. D. Courjon and C. Bainier, "Near field microscopy and near field optics," Rep. Prog. Phys. **57**(10), 989–1028 (1994).
5. D. Courjon, *Near Field Microscopy and Near Field Optics* (Imperial College Press, 2003)
6. B. Prade and J. Y. Vinet, "Guided optical waves in fibers with negative dielectric constant," J. Lightwave Technol. **12**(1), 6–18 (1994).
7. L. Novotny and C. Hafner, "Light propagation in a cylindrical waveguide with a complex, metallic, dielectric function," Phys. Rev. E Stat. Phys. Plasmas Fluids Relat. Interdiscip. Topics **50**(5), 4094–4106 (1994).
8. H. Shin, P. B. Catrysse, and S. Fan, "Effect of the plasmonic dispersion relation on the transmission properties of subwavelength cylindrical holes," Phys. Rev. B **72**(8), 085436 (2005).
9. Y. Wang, X. Ma, M. Pu, X. Li, C. Huang, W. Pan, B. Zhao, J. Cui, and X. Luo, "Transfer of orbital angular momentum through sub-wavelength waveguides," Opt. Express **23**(3), 2857–2862 (2015).
10. G. Tsiminis, Y. Wang, P. E. Shaw, A. L. Kanibolotsky, I. F. Perepichka, M. D. Dawson, P. J. Skabara, G. A. Turnbull, and I. D. W. Samuel, "Low-threshold organic laser based on an oligofluorene truxene with low optical losses," Appl. Phys. Lett. **94**(24), 243304 (2009).
11. C. W. Chang, M. Liu, S. Nam, S. Zhang, Y. Liu, G. Bartal, and X. Zhang, "Optical Möbius symmetry in metamaterials," Phys. Rev. Lett. **105**(23), 235501 (2010).
12. C. A. Pfeiffer, E. N. Economou, and K. L. Ngai, "Surface polaritons in a circularly cylindrical interface: surface plasmons," Phys. Rev. B **10**(8), 3038–3051 (1974).

#247550 Received 10 Aug 2015; revised 6 Oct 2015; accepted 27 Oct 2015; published 2 Nov 2015

13. S. J. Al-Bader, M. Imtaar, "Azimuthally uniform surface-plasma modes in thin metallic cylindrical shells," IEEE J. Quantum Electron. **28**(2), 525–533 (1992).
14. J. Takahara, S. Yamagishi, H. Taki, A. Morimoto, and T. Kobayashi, "Guiding of a one-dimensional optical beam with nanometer diameter," Opt. Lett. **22**(7), 475–477 (1997).
15. M. A. Schmidt and P. S. J. Russell, "Long-range spiralling surface plasmon modes on metallic nanowires," Opt. Express **16**(18), 13617–13623 (2008).
16. S. Zhang, H. Wei, K. Bao, U. Håkanson, N. J. Halas, P. Nordlander, and H. Xu, "Chiral surface plasmon polaritons on metallic nanowires," Phys. Rev. Lett. **107**(9), 096801 (2011).
17. C. M. Chen, C. K. Young, K. R. Chen, and Y. C. Lan, "Spiral surface plasmon modes on uniform and tapered metallic nanorods," J. Opt. Soc. Am. B **30**(9), 2529–2534 (2013).
18. L. Gomez, R. Bachelot, A. Bouhelier, G. P. Wiederrecht, S. H. Chang, S. K. Gray, F. Hua, S. Jeon, J. A. Rogers, M. E. Castro, S. Blaize, I. Stefanon, G. Lerondel, and P. Royer, "Apertureless scanning near-field optical microscopy: a comparison between homodyne and heterodyne approaches," J. Opt. Soc. Am. B **23**(5), 823–833 (2006).
19. A. Bek, R. Vogelgesang, and K. Kern, "Apertureless scanning near field optical microscope with sub-10 nm resolution," Rev. Sci. Instrum. **77**(4), 043703 (2006).
20. A. F. Oskooi, D. Roundy, M. Ibanescu, P. Bermel, J. D. Joannopoulos, and S. G. Johnson, "MEEP: a flexible free-software package for electromagnetic simulations by the FDTD method," Comput. Phys. Commun. **181**(3), 687–702 (2010).
21. P. B. Johnson and R. W. Christy, "Optical constants of the noble metals," Phys. Rev. B **6**(12), 4370–4379 (1972).
22. A. Yariv, *Optical Electronics in Modern Communications*, 5th ed. (Oxford University Press, 1997).
23. F. Gallego-Gómez, E. M. García-Frutos, J. M. Villalvilla, J. A. Quintana, E. Gutierrez-Puebla, A. Monge, M. A. Díaz-García, and B. Gómez-Lor, "Very large photoconduction enhancement upon self-Assembly of a new triindole derivative in solution-processed films," Adv. Funct. Mater. **21**(4), 738–745 (2011).

1. Introduction

Surface plasmons (SPs) that propagate inside metallic nanoholes have drawn a lot of research interests because they are closely related to the extraordinary optical transmission of a thin metallic film with sub-wavelength hole arrays [1–3]. They also play a key role in the probing tip of a near-field scanning optical microscopy (NSOM) [4, 5]. Various SP eigenmodes that propagate inside a cylindrical nanohole drilled in a metallic film have been derived and identified [6–9]. The fundamental SP mode is the HE_1 mode, whose dispersion relation ($\omega - k$ diagram) crosses the light line and is divided into the fast-wave branch and slow-wave branch for they lying to the left and right, respectively, of light line [6]. The HE_1 mode is generally adopted in NSOM tip as a main propagation mode. However, when probing the optical behavior of chiral molecules [10] or chiral metamaterials [11], the HE_1 mode is inconvenient for its polarization direction mismatching with the analytes. In this situation, a possible "spiral surface plasmon" (SSP) mode with special handedness inside the metallic nanohole is required.

The complementary structures of metallic nanoholes, i.e. the metallic nanorods, also support SP modes on their surface [6, 12–14]. However, all the SP modes belong to the slow-wave branch. Recently, the SSP modes that surround the metallic nanorods have been reported [15–17]. Such special modes are formed by linearly superposing two rotating SP eigenmodes of metallic nanorods. The chirality, the number of strands and the spiral pitch of the SSP mode are determined by the properties of the component SP eigenmodes. A tapered nanorod is often used as a scanning tip in the apertureless NSOM [18, 19]. The SSP modes also appear on the tapered nanorod with the spiral pitch decreasing with the reduction of the nanorod radius [17]. However, because of the impedance mismatch on the tapered nanorod, the scattering loss causes a substantial decline in the field energy intensity on the tip of the nanorod.

In this paper, the SSP modes inside a cylindrical nanohole with the metallic surface are proposed and investigated. The single- and triple-stranded SSP modes that are composed of the rotating SP eigenmodes of the fast-wave branch inside the metallic nanohole are demonstrated by FDTD simulation. The SSP modes inside the tapered metallic nanoholes are also explored. The changes of spiral pitch and field energy density of SSP modes with the propagation position are observed and elucidated. Finally, the propagation of SSP modes inside a tapered metal-clad fiber capped by a tapered metallic nanorod is examined. In this composite structure, the SSP mode inside the lower metal-clad fiber is transformed into the SSP mode on the upper metallic nanorod. However, the handedness of SSP mode on the upper metallic nanorod is

#247550 Received 10 Aug 2015; revised 6 Oct 2015; accepted 27 Oct 2015; published 2 Nov 2015

reversed to that inside the lower metal-clad fiber. Furthermore, the field energy density of SSP mode that arrives at the tip of the tapered nanorod is largely increased by using this composite structure.

The rest of this paper is organized as follows. Section 2 describes the simulation structure and method. Section 3 then presents the analyses of SP eigenmodes inside a uniform metallic nanohole. Next, Section 4 presents and discusses the results. Conclusions are finally drawn in Section 5.

2. Simulation structure and method

Figure 1(a) plots the simulated cylindrical nanohole that is drilled in the center of a square silver (Ag) plate. The radius of the nanohole (a) is set to 250 nm. The transverse size of the Ag plate is 800 nm. The length of the nanohole is long enough to observe a few complete spiral patterns. Figure 1(b) presents the simulated tapered cylindrical nanohole inside a square Ag plate. The radii of lower and upper bases of the nanohole are 300 nm and 165 nm, respectively. The transverse size of the Ag plate is also 800 nm. The length of the tapered nanohole is 12500 nm. Both in Figs. 1(a) and 1(b), the nanoholes are filled with the matching transparent medium of permittivity of 2.25. Figure 1(c) plots the simulated tapered Ag-clad fiber with a uniform core and capped by a tapered Ag nanorod. The radius of the dielectric core is 165 nm. The outer radii of the lower and upper bases of the tapered Ag cladding are 300 nm and 192.7 nm, respectively. The length of the tapered section is 3450 nm. (The length of the lower uniform section is 1300 nm.) For the tapered Ag nanorod cap, the lower radius, the upper radius and the length are 192.7 nm, 20 nm and 5550 nm, respectively. The relative permittivity of the fiber core is 2.25. Figure 1(d) presents the simulated tapered Ag nanorod, which is the same structure as Fig. 1(c) except that the material of the uniform core is also Ag.

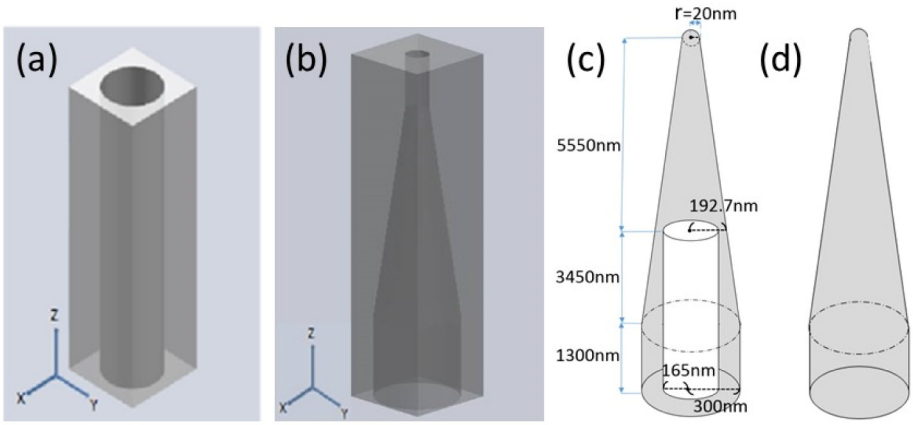

Fig. 1. Simulated structures: (a) uniform Ag nanohole, (b) tapered Ag nanohole, (c) tapered Ag-clad fiber with a uniform core and capped by a tapered Ag nanorod, and (d) tapered Ag nanorod.

The three-dimensional FDTD program MEEP is applied to perform the simulation [20]. The Cartesian x-y-z coordinate system is used (the axis of nanohole is along the z-direction). For Figs. 1(a)-1(d), both the x and y dimensions of the grid cell are 5 nm. The z dimension of the grid cell is 10 nm. The surrounding boundaries are perfectly matched layers. The Drude model of Ag is used with the plasma frequency and collision frequency set to $1.32\times10^{16}\ rad/s$ and $0.68\times10^{14}\ rad/s$, respectively [17, 21]. To excite TM_0 SP eigenmode inside the nanohole, the Ez-polarized plane wave is normally incident into the base of the nanohole. The HE_1 mode is excited by combining an Ex-polarized plane wave and an Ey-polarized plane wave with a phase difference of $\pi/2$ between them (i.e. the circularly-polarized plane wave) and normally

#247550 Received 10 Aug 2015; revised 6 Oct 2015; accepted 27 Oct 2015; published 2 Nov 2015

incident into the base of the nanohole. To excite HE_2 mode, two circularly-polarized plane waves that are modulated by the space functions $\cos\theta$ and $\sin\theta$ (θ is the azimuth angle in the cylindrical coordinate system), respectively, with a phase difference of $\pi/2$ between them are also normally incident into the base of the nanohole. Experimentally, injecting the single mode (HE_{11} and HE_{21}) VCSELs light source into the fiber tip and approaching the Ag nanohole can excite the respective (HE_1 and HE_2) mode in the nanohole.

3. Analyses of SP eigenmodes inside a uniform metallic nanohole

In the cylindrical coordinate system, the z-components electric field (E_z) and magnetic field (H_z) of the rotating SP eigenmode inside the hole ($r < a$) and outside the hole ($r > a$) are express as [6, 17, 22]:

for $r < a$:

$$\begin{aligned} E_z &= C_n\, I_n(\alpha_d r)\, e^{i(\pm n\theta - \beta z + \omega t)} \\ H_z &= D_n\, K_n(\alpha_d r)\, e^{i(\pm n\theta - \beta z + \omega t)} \end{aligned} \tag{1}$$

for $r > a$:

$$\begin{aligned} E_z &= C_n \frac{I_n(\alpha_d a)}{K_n(\alpha_m a)} K_n(\alpha_m r)\, e^{i(\pm n\theta - \beta z + \omega t)} \\ H_z &= D_n \frac{I_n(\alpha_d a)}{K_n(\alpha_m a)} K_n(\alpha_m r)\, e^{i(\pm n\theta - \beta z + \omega t)} \end{aligned} \tag{2}$$

where C_n and D_n are the amplitude coefficients; I_n and K_n denote the modified Bessel functions of the first and second kinds, respectively; n is the mode number; ω is the angular frequency of the eigenmode; $\alpha_d = \sqrt{\beta^2 - k_0^2 \varepsilon_d}$, $\alpha_m = \sqrt{\beta^2 - k_0^2 \varepsilon_m}$; β and k_0 are the wavevectors in the nanohole and in free space, respectively; and ε_d (ε_m) denotes the relative permittivity of dielectric material inside the hole (metal). Substituting Eqs. (1) and (2) into Maxwell's equations and applying the boundary conditions at the dielectric-metal interface, the dispersion relations of the SP eigenmodes with different n's values are acquired as

$$\begin{aligned} &\frac{n^2}{a^2}\left(\frac{\varepsilon_m}{\alpha_m^2} - \frac{\varepsilon_d}{\alpha_d^2}\right)\left(\frac{1}{\alpha_m^2} - \frac{1}{\alpha_d^2}\right) = \\ &\left[\frac{k_n'(\alpha_m a)}{\alpha_m k_n(\alpha_m a)} - \frac{I_n'(\alpha_d a)}{\alpha_d I_n(\alpha_d a)}\right]\left[\frac{\varepsilon_m}{\alpha_m}\frac{k_n'(\alpha_m a)}{k_n(\alpha_m a)} - \frac{\varepsilon_d}{\alpha_d}\frac{I_n'(\alpha_d a)}{I_n(\alpha_d a)}\right] \end{aligned} \tag{3}$$

The dispersion curves for the first three SP eigenmodes (n = 1 (HE_1), 0 (TM_0) and 2 (HE_2)) with $a = 250\,nm$ are plotted in Fig. 2(a) (the material parameters, ε_d and ε_m, are given in Sect. 2). Figure 2(a) exhibits that these SP eigenmodes cross the light line and are divided into the fast-wave and slow-wave branches for their dispersion curves lying to the left- and right-side, respectively, of the light line. Furthermore, the dispersion curves of the slow-wave branches approach one another. It implies that for a fixed frequency, the differences in β's values between the SP eigenmodes become very small. Figures 2(b) and 2(c) plot the simulated instant E_z contours in the x-y plane for the fast-wave branches of HE_1 (dipole-like mode) and HE_2 (quadruple-like mode), respectively, at $\lambda_0 = 633\,nm$ (λ_0 denotes the incident wavelength, $a = 250\,nm$). At a specific time t, these two modes rotate clockwise or counterclockwise along + z direction when the phase terms in Eqs. (1) and (2) take $-n\theta$ or $+n\theta$, respectively. (TM_0 is independent of θ, i.e. $n = 0$ in Eqs. (1) and (2).)

#247550 Received 10 Aug 2015; revised 6 Oct 2015; accepted 27 Oct 2015; published 2 Nov 2015

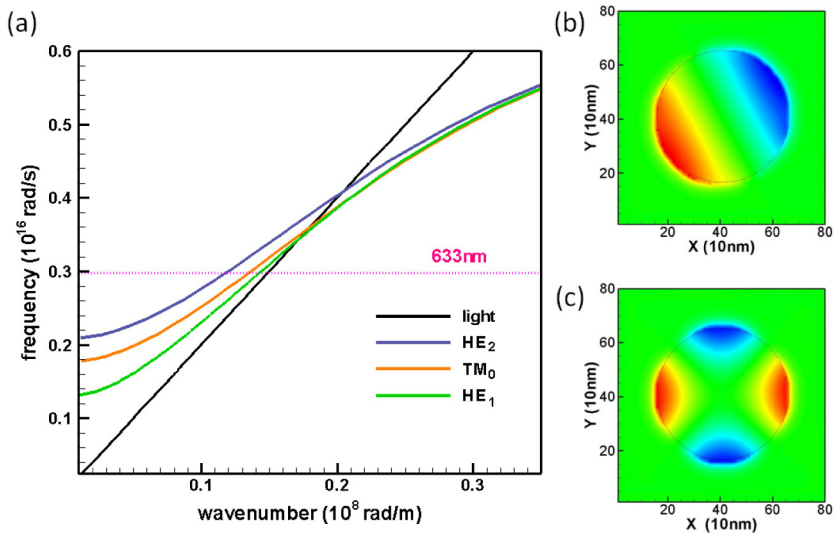

Fig. 2. (a) Dispersion relations (frequency vs. wavevector) for HE_1, TM_0 and HE_2 SP eigenmodes inside a uniform Ag nanohole with a = 250 nm and filled with the medium of permittivity of 2.25. (b) and (c) Simulated instant E_z contours in x-y plane for the fast-wave branches of HE_1 and HE_2, respectively. (with a = 250 nm and λ_0 = 633 nm)

Notably, in solving the dispersion relation of SP eigenmode (Eq. (3)), the metallic loss is neglected. When the metallic loss is considered, β's value becomes a complex number. However, the real part of β's value remains almost unchanged. Hence the properties of the SSP mode also remain unchanged. The imaginary part of β's value only causes the intensity of SSP mode to decay along z direction.

4. Results and discussion

The SSP modes inside the uniform Ag nanohole are explored first. The SSP modes are formed by combining two different SP eigenmodes in the fast-wave branches. Figure 3(a) plots the simulated time-averaged contour of magnetic field (H-field) energy density in three-dimensional space for the incident counterclockwise ($+\theta$ in Eqs. (1) and (2)) HE_1 mode and counterclockwise ($+2\theta$ in Eqs. (1) and (2)) HE_2 mode with $a = 250\,nm$ and $\lambda_0 = 633\,nm$. Figure 3(b) presents the same contour in the x-y plane at z = 2880 nm. Here the choice of HE_1 and HE_2 modes instead of HE_1 and TM_0 modes (see Fig. 2(a)) is based on that the former will produce more complicated and interesting spiral patterns. Furthermore, the formation mechanism and spiral pitch of SSP mode can be clearly deduced from the combination of HE_1 and HE_2 modes. Figures 3(a) and 3(b) show that a left-handed single-stranded spiral pattern is formed inside the Ag nanohole. (The handedness is defined by the rotation direction of the spiral pattern along + z direction.) The simulated spiral pitch is about 2613 nm. Figures 3(c) and 3(d) plot the same simulated time-averaged contours of H-field energy density in three-dimensional space and in the x-y plane at z = 2880 nm, respectively, for the incident clockwise ($-\theta$) HE_{-1} mode and counterclockwise ($+2\theta$) HE_2 mode with $a = 250\,nm$ and $\lambda_0 = 633\,nm$. Figures 3(c) and 3(d) reveal that the left-handed triple-stranded spiral patterns are produced inside the Ag nanohole. The simulated spiral pitch is about 7780 nm. Figures 3(a) and 3(c) also indicate that the number of strands of SSP modes is determined by the relative rotation directions of the two component modes.

#247550 Received 10 Aug 2015; revised 6 Oct 2015; accepted 27 Oct 2015; published 2 Nov 2015

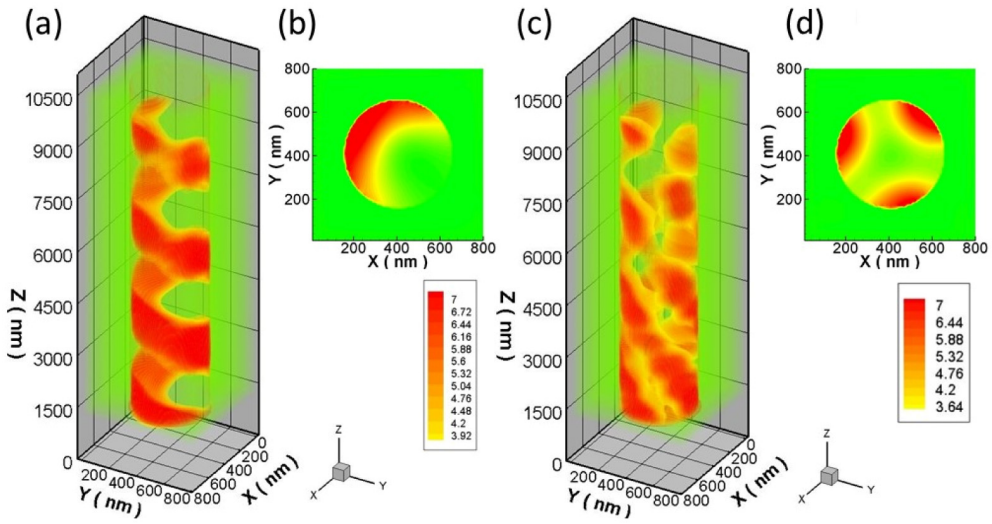

Fig. 3. (a) and (b) Simulated time-averaged contours of H-field energy density in three-dimensional space and in x-y plane at z = 2880 nm, respectively, for incident counterclockwise HE_1 mode and counterclockwise HE_2 mode. (c) and (d) Simulated time-averaged contours of H-field energy density in three-dimensional space and in x-y plane at z = 2880 nm, respectively, for incident clockwise HE_{-1} mode and counterclockwise HE_2 mode. (The structure is shown in Fig. 1(a), a = 250 nm and λ_0 = 633 nm)

The formation of SSP mode inside an Ag nanohole is further investigated. The total z-component magnetic field Ψ of the combined $HE_{\pm 1}$ (rotating counterclockwise or clockwise) and HE_2 (rotating counterclockwise) modes is

$$\psi = R_{\pm 1}(r)e^{i(\pm\theta-\beta_1 z+\omega t)} + R_2(r)e^{i(2\theta-\beta_2 z+\omega t+\phi_0)} \tag{4}$$

where $R_{\pm 1}(r)$ and $R_2(r)$ represent the *r*-dependent functions in Eqs. (1) and (2), and ϕ_0 is the phase difference between $HE_{\pm 1}$ and HE_2 modes. The time-averaged H-field energy density is proportional to

$$|\psi|^2 = |R_{\pm 1}(r)|^2 + |R_2(r)|^2 + 2|R_{\pm 1}(r)||R_2(r)|\cos[(\beta_1-\beta_2)z + m\theta + \phi_0'] \tag{5}$$

where m = 1 and m = 3 for the first term of Eq. (4) to take $+\theta$ and $-\theta$, respectively; ϕ_0' equals to $\varphi_0 + \arg(R_{\pm 1}(r)) - \arg(R_2(r))$, and arg is to take the argument of a complex number. Equation (5) represents a left-handed (due to the $+m\theta$ term in cos function) single-stranded (m = 1) or triple-stranded (m = 3) spiral pattern along the z-axis, as shown in Figs. 3. The spiral pattern originates in beating of $HE_{\pm 1}$ and HE_2 SP eigenmodes. The spiral pitch, L_{sp}, is obtained from $L_{sp} = m2\pi/(\beta_1-\beta_2)$ (Eq. (5)). Using it, the calculated spiral pitches for single-stranded and triple-stranded SSP modes are 2545 nm and 7635 nm, respectively. Both of them agree with the simulation results well. Equation (5) also implies that the right-handed SSP mode will be produced when using HE_{-2} (clockwise, -2θ) mode. Furthermore, the single-stranded (double-stranded) SSP modes can be produced by a superposition of $HE_{\pm 1}$ and TM_0 (TM_0 and $HE_{\pm 2}$) component modes.

Theoretically, the SSP modes can also be made up of the slow-wave branches of the SP eigenmodes. However, in our simulation model, since the differences in β's values between the slow-wave branches of SP eigenmodes are very small, the spiral pitch will become very large. Moreover, the waveguide modes inside the Ag nanohole also possibly interfere with the

#247550 Received 10 Aug 2015; revised 6 Oct 2015; accepted 27 Oct 2015; published 2 Nov 2015

SP modes. Therefore, the SSP modes that consist of the slow-wave branches of the SP eigenmodes cannot be observed in the simulation.

The changes of spiral pitch of SSP mode with the nanohole radius and the incident wavelength are also examined. Figure 4(a) plots the calculated spiral pitches as a function of nanohole radius for λ_0 = 633 nm, 660 nm, and 700 nm (the single-stranded SSP mode is made of HE_1 and HE_2 SP eigenmodes, Fig. 3(a)). (The calculated spiral pitches are obtained from $L_{sp} = 2\pi/(\beta_1 - \beta_2)$, where β_1 and β_2 are the wavevectors of HE_1 and HE_2, respectively, modes and are acquired by solving Eq. (3)). The FDTD simulated spiral pitches for $\lambda_0 = 633\,nm$ are also shown for comparison. Figure 4(a) exhibits that, for a fixed incident wavelength, the spiral pitch increases with the nanohole radius. This result implies that the spiral pitch of SSP mode gradually decreases in the tapered nanohole. Figure 4(b) presents the calculated and simulated spiral pitches versus the incident wavelength for the same SSP mode as in Fig. 4(a) with $a = 250\,nm$. Figure 4(b) indicates that the spiral pitch of SSP modes is inversely related to the incident wavelength. This result is ascribed to that the value of $\beta_1 - \beta_2$ increases with the wavelength, as shown in Fig. 2(a).

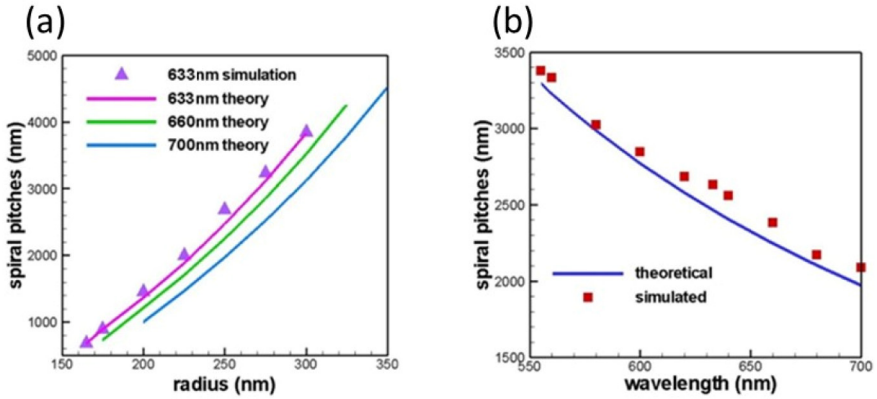

Fig. 4. (a) Calculated and simulated spiral pitches as a function of nanohole radius for different incident wavelengths. (b) Calculated and simulated spiral pitches vs. incident wavelength with a = 250 nm. The SSP mode is the same as in Fig. 3(a).

Next, the behavior of SSP mode inside the tapered Ag nanohole is also examined. Here the SSP mode is made of counterclockwise HE_1 mode and counterclockwise HE_2 mode (i.e. the left-handed single-stranded SSP mode). Figure 5(a) plots the simulated time-averaged contour of H-field energy density in three-dimensional space for the SSP mode with the structure shown in Fig. 1(b) and $\lambda_0 = 633\,nm$. Figure 5(a) displays that the spiral pitch decreases with the reduction of nanohole radius in the tapered region, which agrees with the calculated results shown in Fig. 4(a). Figure 5(b) presents the θ-integrated H-field energy density on the inner surface of the tapered nanohole as a function of z. It reveals that the H-field energy density along z increases to a maximum value (at about $z = 10400\,nm$ where $a = 196\,nm$) and then falls significantly at the end of the tapered region. The field energy density increasing with z is caused by that the field energy is concentrated in smaller regions when the nanohole radius decreases. However, because of the impedance mismatch at the junction of the tapered and uniform sections (which is not adiabatic), the reflection of SP eigenmodes (which are excited around the junction) inside the nanohole leads to the fall in field energy finally. (The decline in field energy at the entrance of the tapered region is due to the same reason.)

#247550 Received 10 Aug 2015; revised 6 Oct 2015; accepted 27 Oct 2015; published 2 Nov 2015

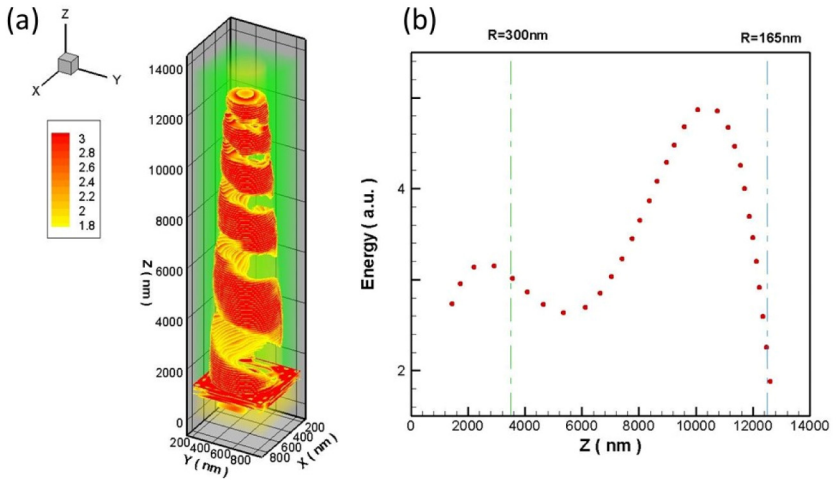

Fig. 5. (a) Simulated time-averaged contour of H-field energy density in three-dimensional space for SSP mode propagating inside a tapered Ag nanohole. (b) θ-integrated H-field energy density on the inner surface of the tapered nanohole as a function of z. The SSP mode is the same as in Fig. 3(a) with λ_0 = 633 nm.

Finally, the propagation of SSP modes inside a tapered Ag-clad fiber with a uniform core and capped by a tapered Ag nanorod is examined. The simulated geometry has been depicted in Fig. 1(c). In this investigation, the SSP mode is composed of counterclockwise HE_1 mode and TM_0 mode. (TM_0 and HE_1 modes are the first two SP eigenmodes of the upper Ag nanorod [17].) Figs. 6(a) and 6(b) plot the simulated time-averaged contours of H-field energy density in three-dimensional space for the SSP mode inside the lower tapered Ag-clad fiber and on the upper tapered Ag nanorod, respectively. Notably, because the field amplitude of SSP modes is largely reduced when the field tunnels into the upper tapered Ag nanorod from the lower Ag-clad fiber via evanescent field coupling between them, the contour levels in Fig. 6(b) are rescaled to emphasize the field patterns on the upper tapered Ag nanorod. Figure 6(a) reveals that the SSP mode inside the fiber is right-handed and single-stranded. Contrarily, Fig. 6(b) shows that, the handedness of the SSP mode on the upper tapered Ag nanorod is reversed to that inside the lower fiber (i.e. the SSP mode on the upper Ag nanorod is left-handed).

The above phenomenon can be elucidated by analyzing the dispersion relations of the SP eigenmodes inside the Ag nanohole and on the Ag nanorod. Figure 6(c) presents the calculated HE_1 and TM_0 SP eigenmodes inside the Ag nanohole with the radius of 160 nm (close to the radius of the fiber core in Fig. 1(c)) and on the Ag nanorod with the radius of 192.7 nm (equal to the lower radius of the capped tapered nanorod in Fig. 1(c)). Figure 6(c) exhibits that inside the Ag nanohole, the lowest fast-branch SP eigenmode is HE_1 mode and then TM_0 mode. Conversely, on the Ag nanorod, the SP eigenmodes lie to the right of light line and follow the order of TM_0 mode and HE_1 mode. For incident counterclockwise HE_1 mode and TM_0 mode ($\lambda_0 = 633\ nm$), the equal-phase condition of the time-averaged H-field energy density of the SSP mode is $(\beta_1 - \beta_0)z - \theta = constant$ (see the cos function in Eq. (5)). (Here β_1 and β_0 represent the wavevectors of HE_1 mode and TM_0 mode, respectively.) For SSP mode inside the Ag-clad fiber, $(\beta_1 - \beta_0) > 0$ and the time-averaged H-field energy density represents a right-handed single-stranded spiral pattern along the z-axis (due to $-\theta$ term), which agrees with the simulation result shown in Fig. 6(a). On the contrary, for SSP mode on the Ag nanorod, $(\beta_1 - \beta_0) < 0$ and the equal phase condition becomes $(\beta_0 - \beta_1)z + \theta = constant$. Then the time-averaged H-field energy density displays a left-handed single-stranded spiral pattern

#247550 Received 10 Aug 2015; revised 6 Oct 2015; accepted 27 Oct 2015; published 2 Nov 2015

along the z-axis (due to $+\theta$ term), as shown in Fig. 6(b). Therefore, the SSP mode changes its handedness when the field tunnels into the tapered Ag nanorod from the tapered Ag-clad fiber.

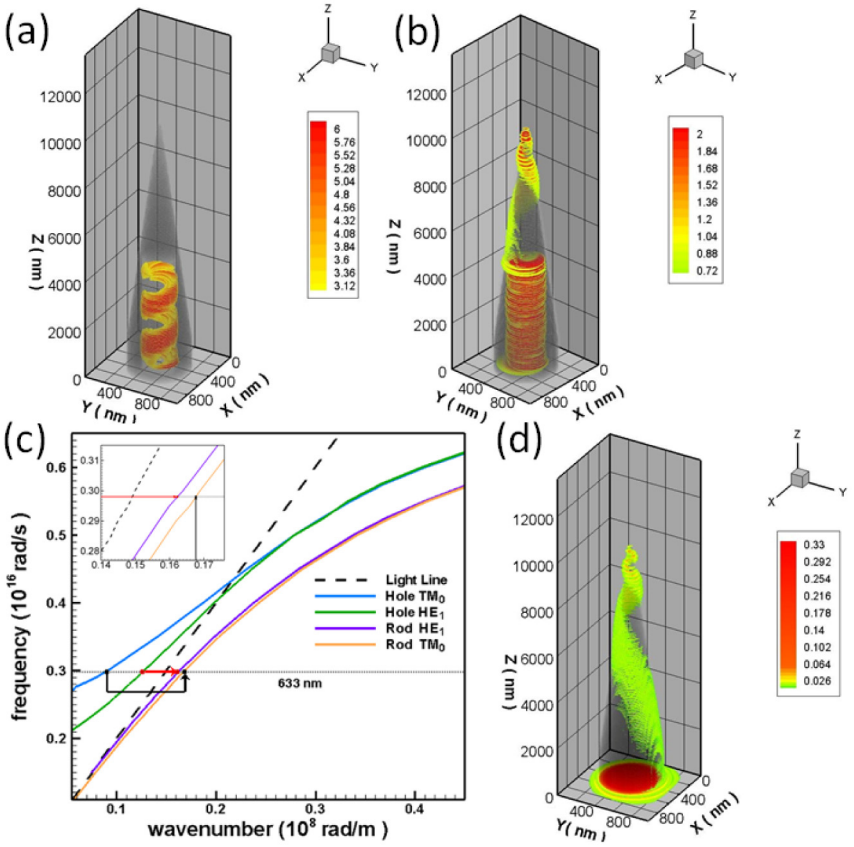

Fig. 6. (a) and (b) Simulated time-averaged contours of H-field energy density in three-dimensional space for SSP mode inside the tapered Ag-clad fiber and on the upper tapered Ag nanorod, respectively. (c) Dispersion relations for HE_1 and TM_0 SP eigenmodes inside a uniform Ag nanohole with the radius of 160 nm and on a uniform Ag nanorod with the radius of 192.7 nm. (The relative permittivity of fiber core is 2.25). Inset: Enlargement of dispersion curves of SP eigenmodes on the uniform Ag nanorod around λ_0 = 633 nm. (d) Simulated time-averaged contours of H-field energy density in three-dimensional space for SSP mode on the tapered Ag nanorod. In (a), (b) and (d), the SSP mode is composed of counterclockwise HE_1 mode and TM_0 mode with λ_0 = 633 nm.

Figure 6(d) plots the simulated time-averaged contours of H-field energy density in three-dimensional space for SSP mode on the tapered Ag nanorod (Fig. 1(d)). Notably, the simulated input components and powers for Figs. 1(c) and 1(d) are the same. Figure 6(d) shows that the SSP mode can also propagate on the simulated tapered nanorod. However, comparing with Fig. 6(b), the time-averaged H-field energy density at the tip for the structure of Fig. 1(d) is much smaller than that for the structure of Fig. 1(c). This result implies that the field energy density of SSP mode at the tip of the nanorod is largely increased by using the composite structure of Fig. 1(c). It is ascribed to that more power of SSP mode is allowed to propagate inside the Ag-clad fiber than on the Ag nanorod.

The SSP mode inside a metallic nanohole can be applied to NSOM tip for probing the molecules and metamaterials with special symmetry. For example, the triple-stranded SSP

#247550 Received 10 Aug 2015; revised 6 Oct 2015; accepted 27 Oct 2015; published 2 Nov 2015

mode is more convenient to explore C_3-symmetry molecules, such as truxene derivatives and triindole derivatives [10, 23], and C_3-symmetry trimer metamolecular [11].

5. Conclusion

The SSP modes that propagate inside an Ag nanohole are explored by performing both FDTD simulations and theoretical analyses. The SSP modes are formed by combining two rotating SP eigenmodes of the Ag nanohole in the fast-wave branches. Inside a uniform Ag nanohole, the handedness (left-handed or right-handed) and the number of strands of the SSP modes are determined by both the component SP eigenmodes (e.g. HE_1, TM_0 and HE_2) and their rotation directions (clockwise or counterclockwise). Furthermore, the spiral pitch increases with the nanohole radius for a fixed wavelength and is inversely related to the incident wavelength for a fixed nanohole radius. For the SSP mode propagating inside a tapered Ag nanohole, the spiral pitch decreases with the reduction of nanohole radius in the tapered region, which agrees with the calculated results. However, the azimuth-integrated field energy density increases to a maximum value and then falls. Finally, considering a tapered Ag-clad fiber capped by a tapered Ag nanorod, the SSP mode reverses its handedness when it passes through the fiber-nanorod interface. Moreover, the field energy density of the SSP mode that arrives at the tip of the nanorod is largely increased by using this composite structure. The SSP mode inside a metallic nanohole can be applied to NSOM tip for probing the molecules and metamaterials with special symmetry.

Acknowledgment

This work was supported by the Ministry of Science and Technology of Taiwan under Contract Nos. 101-2112-M-006-002-MY3, 104-2112-M-006-005-MY3, 103-2221-E-009-076 and 104-2221-E-009- 155-MY3. National Center for High-Performance Computing of Taiwan is also acknowledged for uses of facilities.

#247550 Received 10 Aug 2015; revised 6 Oct 2015; accepted 27 Oct 2015; published 2 Nov 2015